Chapter 3

GMRT H I imaging of galaxies in X-ray bright groups

Environment plays an important role in the evolution of the gas contents of galaxies. Gas deficiency of cluster spirals and the role of the hot intracluster medium (ICM) in stripping gas from these galaxies is a well studied subject. Loose groups with diffuse X-ray emmision from the intragroup medium (IGM) offer an intermediate environment between clusters and groups without a hot IGM. These X-ray bright groups have smaller velocity dispersion and lower temperature than clusters, but higher IGM density than loose groups without diffuse X-ray emission. The single dish comparative study of loose groups with and without diffuse X-ray emission from the IGM, discussed in the Chapter One of this thesis, showed that the galaxies in X-ray bright groups have lost more gas on average than the galaxies in non X-ray bright groups. In this chapter, we present GMRT H I observations of 13 galaxies from 4 X-ray bright groups: NGC5044, NGC720, NGC1550 and IC1459. The aim of this work is to study the morphology of H I in these galaxies and to see if the hot IGM has in any way affected their H I content or distribution.

3.1 Introduction

Galaxies are found in different environments like field, loose groups, compact groups and clusters. The environment plays an important role in the gas contents of galaxies. A range of gas removal processes work in these environments. Depending on the position of the galaxy in the group or in the cluster, the galaxy looses gas to the environment to different degrees. Spiral galaxies in cluster cores are well known to be atomic hydrogen (H I) deficient. They move through the dense hot cluster cores with high velocities and lose gas through ram pressure stripping [58]. The hot (10^8 K) intracluster medium (ICM) can also strip gas from the galaxy through evaporation [34]. Detailed observations have been carried out over the past three decades to probe gas deficiency in cluster galaxies. They seem to suggest that a large fraction of the cluster galaxies are actually deficient in H I . More deficient galaxies are found closer to the cluster centre and many galaxies have truncated or shrunken H I disks or extraplanar gas indicating ram pressure stripping ([59], [24], [36]).

While cluster galaxies have been extensively studied, not many studies exist about the gas content and gas deficiency of the galaxies in groups and the possible gas removal processes that can succesfully work in such environments. Compact groups have been studied better than loose groups. A sample of 72 HCGs were studied with single dish and a subset of those with the VLA. The galaxies in the HCGs were found to be H I deficienct by greater than a factor of 2 on an average. Some of these groups have been detected in X-rays and the X-ray detection rate is found to be higher for the H I deficient groups [155].

H I content and deficiency studies of loose groups are not so well reported in literature. H I deficiency by a factor of more than 1.6 has been reported in some members of a loose group in the Puppis region [29]. Galaxies in Eridanus, a large loose group, have been found to be H I deficient by a factor of 2 to 3. About 31 galaxies from the Eridanus group have been imaged in H I using the Giant Meterwave Radio Telescope (GMRT). From these images and the overall group properties, tidal interaction was found to be the most likely gas removal

mechanism responsible for the H I deficiency of Eridanus galaxies [102].

Ram pressure becomes an effective gas removal process only when the H I surface mass density is less than $\rho_0 v^2/(2\pi\ G\sigma_*)$, where σ_* is the stellar surface mass density. So, larger the intra-cluster medium (ICM) density, ρ_0, and galaxy velocity, v, the more effective is this stripping. Thus in the absence of a hot IGM and a high velocity dispersion, tidal interaction appears to be the most favourable process by which galaxies in groups can lose gas, though there are some cases where ram pressure is also acting in groups [78]. Detection of hot intragroup medium (IGM) in some poor groups has presented an intermediate environment between clusters and groups without a hot IGM. When the group has a hot IGM, ram pressure or thermal conduction can contribute significantly to make the galaxies deficient in H I. Since low velocity dispersion in these groups increases the probability of tidal interactions, tidal assisted ram pressure stripping can also contribute to gas loss from galaxies [39]. NGC2276, a spiral in the NGC2300 group is found to be H I deficient and signatures of the hot IGM affecting the galaxy were detected [113]. A comparative single dish study of the H I contents of loose groups with and without the hot IGM indicates that the X-ray emitting medium may play a significant role in removing gas from the galaxies, as galaxies in these groups are found to be more H I deficient than the galaxies in groups without X-rays [125]. Thus it is interesting to study the H I contents and morphologies of galaxies in groups with a hot IGM, to see if IGM assisted stripping has left its signatures in the H I distribution of the galaxies.

In this chapter, we present GMRT H I images of nine spiral galaxies in four groups whose IGM is detected in X-rays. The aim of this work is to study the morphology of H I in these galaxies and to see if the hot IGM has in any way affected their H I content and distribution.

3.2 GMRT observations and Data analysis

Thirteen galaxies from four groups, where the IGM has been detected in X-rays, were observed with GMRT in the H I 21cm line. The four groups from which this sample of thirteen galaxies were drawn are NGC5044, NGC1550, NGC720 and IC1459. They have a varied

range of X-ray properties (Table 1). NGC5044 is a well studied bright X-ray group with the diffuse emission being mostly circular in morphology with concentric isophotes [19]. NGC1550 is amongst the brightest X-ray groups so far observed and has more relaxed X-ray morphology, except some asymmetries near the group centre, than the other > 1keV groups like NGC5044 [139]. NGC720 and IC1459 are moderately bright groups and are also comparatively nearer than the other two. All the groups have memberships ~ 10 to 20 and have at least one bright elliptical galaxy at their X-ray centres. GMRT H I observations of thirteen galaxies from these four groups are presented in this work. Table 1 lists the group names, their distances, X-ray luminosities and temperatures of the IGM and the number of galaxies observed with the GMRT.

GMRT is an interferometric array of 30 antennas, each of 45m diameter, spread over a maximum baseline of 25 km. At frequencies of ~ 1400 MHz, the system temperature and the gain (K/Jy) of the instrument are 76K and 0.22 respectively. The full width at half maximum of the primary beam of GMRT antennas in L band (frequency 1.4 MHz) is $24'$. The FX correlator of GMRT offers a total of 128 channels for spectral line observations in the full polar mode. The sources selected have a wide range in H I content. The motivation was to study if there were any evidance of the hot IGM being responsible for gas loss from these galaxies. All the sources are below $5'$ in optical size, their distances are between 20 to 60 Mpc, and their declinations range from -36 ° to +02 °. With GMRT they were studied at a spatial resolution of ~3 kpc, a velocity resolution of ~13 km/s and to a H I column density of ~ 1×10^{20} per cm^2. Table 2 lists the relevant details of the observations carried out with the GMRT.

Data obtained with the GMRT were reduced using AIPS (Astronomical Image Processing System). The procedure used to get the total H I maps and the velocity fields is the following. Bad data (dead antennas, antennas with significantly lower gain than others, RFI) were flagged and the data was calibrated for amplitude and phase using standard primary and secondary calibrators. The spectral responses of the filters were corrected by calibrating the data using a standard primary calibrator or when available a strong secondary calibrator.

The calibrated data were used to make both the H I line images and the 20 cm radio continuum images. The continuum data set were prepared from the calibrated data using the line (H I emission) free channels (frequencies). The data were then averaged in frequency and self calibrated. AIPS task 'IMAGR' was then used to get the deconvolved high resolution contunuum images. For the H I line images the calibrated data were continuum subtracted using AIPS tasks 'UVSUB' (used to subtract a model, in this case the clean components from the continuum image, from the uv data) and 'UVLIN' (used to subtract continuum by making linear fits to the uv data). The task 'IMAGR' was then used to get the final 3 dimensional deconvolved H I data cubes. From these cubes the total H I images and the H I velocity fields were extracted using the AIPS task 'MOMNT'. By definition the total H I maps are the integrated flux density maps,

$$I_{tot}(\alpha, \delta) = \triangle \mathrm{v} \sum_{\mathrm{i=1}}^{\mathrm{Nchan}} \mathrm{S}_{\nu}(\alpha, \delta, \nu_{\mathrm{i}}) \tag{3.1}$$

and the velocity fields are the intensity-weighted first order moment of the H I distribution at different velocities.

$$\overline{\mathrm{v}} = \frac{\sum_{\mathrm{i=1}}^{\mathrm{Nchan}} \mathrm{v_i}\ \mathrm{S}_{\nu}(\alpha, \delta, \nu_{\mathrm{i}})}{\sum_{\mathrm{i=1}}^{\mathrm{Nchan}} \mathrm{S}_{\nu}(\alpha, \delta, \nu_{\mathrm{i}})} \tag{3.2}$$

Here $S_{\nu}(\alpha, \delta, \nu_i)$ is the observed flux density at the position (α ,δ) in channel i (which has frequency ν_i and velocity v_i, $\triangle$v is the velocity resolution of the channels and is a constant for a particular dataset and Nchan is the total number of channels over which the H I line exists. The total H I maps were produced at an angular resolution of 15″ to 25″ depending upon the distance to the galaxies, so that the H I morphology could be studied at ∼3 to 4 kpc resolution. Some of the velocity fields were produced at similar resolutions of 15″ to 25″ and some were at lower resolutions (listed in table 2.). The total H I and the velocity fields overlaid on the respective optical images of all the H I detected galaxies are presented. The rms per channel of the line cubes and the synthesised beam sizes are listed in table 2. The units of total H I maps have been converted from Jy m/s (the original map unit) to H I column

densities using the formula,

$$N(HI) = \frac{1.1 \times 10^{21}\ cm^{-2}}{\theta_a \times \theta_b} \triangle \mathrm{v} \sum_{\mathrm{i}=1}^{\mathrm{Nchan}} \mathrm{S}_{\nu}(\alpha, \delta, \nu_{\mathrm{i}}) \tag{3.3}$$

where θ_a and θ_b are the major and minor axes of the synthesised beam in arcseconds, $\triangle$v is the velocity resolution of the channels in km/s and $S_{\nu}(\alpha, \delta, \nu)$ is the H I flux density at the position (α, δ) in the channel i in mJy.

3.3 Results

3.3.1 H I content and deficiency

The total H I maps of the nine H I detected galaxies and their respective velocity fields are presented in Fig 3 - 31. The figure captions contain the galaxy names and the H I column density levels plotted (in total H I maps) or the H I velocity contours (in the H I velocity field maps) and the velocity channel maps for each galaxy. Following are a set of short notes on each of these nine galaxies.

ARP004 (Fig 3, 4, 5, 6): An irregular galaxy from the NGC720 group. The H I distribution is normal in low resolution (Fig 3) and extremely fragmented in high resolution (Fig 5). But the galaxy is not H I deficient. The ratio of GMRT to single dish flux for this galaxy is 0.7. Velocity field is apparently normal. This galaxy is detected in FIR and not detected in radio 20 cm and has an FIR excess.

DDO015 (Fig 7, 8, 9): A dwarf galaxy from NGC720 group. An extremely H I deficient galaxy. Most part of the western and central regions have depleted H I content. The H I disk is also truncated. The ratio of GMRT to single dish flux for this galaxy is 0.9.

MCG-03-34-04 (Fig 10, 11, 12) : This galaxy belongs to the group NGC5044. Its morphological classification is S0. Normally lenticulars do not contain much H I. But this galaxy has a huge H I mass (from single dish) $\sim 8.0\times 10^9$ $M_{\odot}$. The ratio of GMRT to single dish flux for this galaxy is 0.5. A galaxy of this size and morphological type should contain $\sim$

1.8×10^9 $M_\odot$. This galaxy is detected in 20 cm radio continuum and FIR. About 5.5′ away from this galaxy is NGC4997, which is non-detected in both H I and radio continuum, and 11.8′ away is 2MASX J13085477-1636106, a galaxy which has been detected in H I in this GMRT observation. But since 2MASX J13085477-1636106 is close to the edge of the primary beam, no further study can be done with the present observations. Since S0 galaxies have an uncertainty about their H I content and many galaxies even do not contain any H I, though an H I deficiency has been quoted for MCG-03-34-04 (table4), no gas loss by ram pressure or evaporation has been calculated for this galaxy.

MCG-03-34-41 (Fig 13, 14, 15): A late type spiral from NGC5044 group. The HI disk is truncated compared to normal spirals and the galaxy has moderate H I deficiency. The ratio of GMRT to single dish flux for this galaxy is 1.6. It is FIR detected and radio non-detected and has an FIR excess.

SGC1317.2-1702 (Fig 16, 17, 18): A late type spiral in NGC5044 group. The H I distribution is clumpy. The galaxy is moderately H I deficient with a shrunken H I disk. The ratio of GMRT to single dish flux for this galaxy is 0.7.

SGC 1316.2-1722 (Fig 19, 20, 21): A late type spiral in NGC5044 group. The is an H I deficient galaxy with a shrunken H I disk. About 6.1′ away towards north-west, H I has been detected in another galaxy KDG 220. This is a dwarf galaxy. H I has been detected in this galaxy by GMRT at a velocity of 2470 km/s. Radial velocity of this galaxy was unknown before this observation. Total H I map of SGC 1316.2-1722 also shows KDG 220, in the north-west corner. The ratio of GMRT to single dish flux for this galaxy is 0.8.

UGC3014 (Fig 22, 23, 24): This spiral belongs to NGC1550 group. It is close to NGC1550 in both velocity and coordinate, but not a group member according to [48]. H I distribution has an extension in the eastern side and a shrunken H I disk. Velocity field of this galaxy is normal. This galaxy is detected in radio continuum and FIR. The ratio of GMRT to single dish flux for this galaxy is 1.2.

UGC3004 and UGC3005 (Fig 25, 26, 27, 28) : These two galaxies belong to NGC1550

group. UGC3004 (V_{opt}=3571 km/s) is recognised as a group member, but UGC3005 (V_{opt}=3215 km/s) and UGC3006 (V_{opt}=3664 km/s) are not listed group members [48]. UGC3006 was neither detected in H I nor in radio continuum. UGC3004 and UGC3005 look like interacting galaxies in their total H I maps, but they are actually well seperated in velocity and are probably not interacting. UGC3004 has been previously observed by the VLA in H I and in 6 cm [27]. The spectral index of this galaxy was found to be -1.6. This galaxy is also IRAS detected. UGC3005 is a low surface brightness edge on spiral with normal H I content. The ratio of GMRT to single dish flux for these twp galaxies together is 1.0.

IC5269B (Fig 29, 30, 31) : A barred spiral galaxy from IC1459 group. H I distribution and velocity field is normal. The ratio of GMRT to single dish flux for this galaxy is 0.4.

A possible way to establish whether a galaxy has lost gas is to compare its gas content with that of the field galaxy sample, of the same morphological type. The parameter that measures whether a galaxy has an excess or a lower H I content compared to a field sample, referred to as H I deficiency, is defined as [59],

$$def_{\rm H_I} = log\frac{M_{H_I}}{D_l^2}|_{field} \; - \; log\frac{M_{H_I}}{D_l^2}|_{obs} \tag{3.4}$$

where M_{H_I} is the total H I mass of a galaxy and D_l is the optical major isophotal diameter (in kpc) measured at or reduced to a surface brightness level m_B = 25.0 mag/arcsec^2.

The expected field values of $M_{\rm H_I}/D_l^2$ for various morphological types are taken from [59]. While [59] used the UGC blue major diameters for D_l, in this work RC3 major diameters have been used. A Hubble constant of 75 km s^{-1} Mpc^{-1} has been used throughout the work to get distances to the galaxies from their optical velocities. To take care of the difference in the surface matter densities that result from the use of RC3 diameters, a value of 0.08 [51] has been added to the expected surface matter densities given by [59].

Table 3.1: Groups Observed

Group	Distance (Mpc)	T_X (K)	L_X (erg/s)	galaxies (#)
NGC720	21.5	0.51	7.24×10^{40}	2
NGC1550	48.0	1.37	2.0×10^{43}	4
NGC5044	34.8	1.02	6.45×10^{42}	6
IC1459	23.6	0.63	3.31×10^{40}	1

The H I mass was derived from the integrated flux density using the following formula,

$$M_{\mathrm{H_I}}(M_\odot) = 2.36 \times 10^5 \mathrm{D}^2 \triangle \mathrm{v} \sum_{\mathrm{i=1}}^{\mathrm{Nchan}} \mathrm{S_i} \tag{3.5}$$

where D is the distance to the galaxy in Mpc and $\triangle$v is the velocity resolution in km/s. The integrated flux densities for this purpose were taken from the H I Parkes all sky survey (HIPASS) catalog (if not available in catalog, from the spectra) and for galaxies which had noisy HIPASS spectra, GMRT spectra were used to calculate their H I masses. The H I masses and H I deficiencies for the sample galaxies estimated in the above mentioned way are listed in table 4.

3.3.2 H I diameter to optical diameter ratio

Another way of assessing whether a galaxy has lost gas is by comparing its $D_{H\,i}/D_{25}$ ratio to the average value of this ratio found in spirals and irregulars. $D_{H\,i}/D_{25}$ is the ratio of the H I diameters measured at face-on H I surface density of $1\mathrm{M}_\odot$ per pc^2 to the optical major isophotal diameter measured at or reduced to a surface brightness level m_B = 25.0 mag/arcsec^2. The D_{25} in this section is the same as the D_l of section 3.1. The high resolution (15″ to 20″) total H I maps of the galaxies obtained using AIPS were deprojected using the task 'ELLINT' of GIPSY (Groningen Image Processing System). The resultant H I surface density profiles were then fitted with a gaussian [28] and the H I diameters were then measured at or to an extrapolated face-on H I surface density of $1\mathrm{M}_\odot$ per pc^2. The

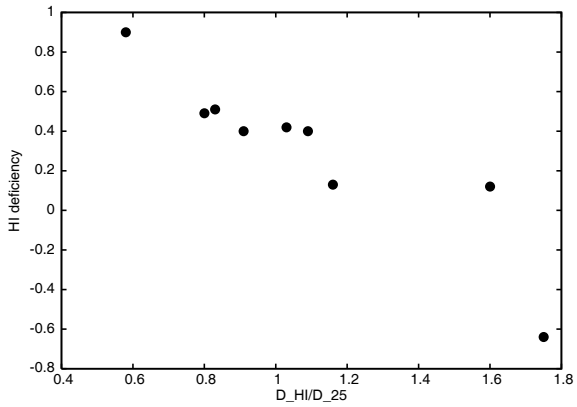

Figure 3.1: H I deficiency plotted against $D_{H\,i}/D_{25}$

values of $D_{H\,i}/D_{25}$ for all the H I detected galaxies are listed in table 4. The high resolution image of ARP004 did not yeild any significant surface density profile and thus the $D_{H\,i}/D_{25}$ value of this galaxy is absent from table 4. They are to be compared with an average value found in spirals and irregulars in fields and groups. [102] and [17] find the average $D_{H\,i}/D_{25}$ value for spirals and irregulars to be 1.7± 0.80 and 1.7± 0.05 respectively. The average value of $D_{H\,i}/D_{25}$ for the eight galaxies in this sample is 1.1±0.12. A plot of H I deficiency against $D_{H\,i}/D_{25}$ for all the galaxies is also presented (Fig. 1). The plot shows decrease in H I deficiency with increasing $D_{H\,i}/D_{25}$.

3.3.3 Radio Continuum

Three of the thirteen galaxies observed with the GMRT were detected in radio continuum. All three had previously been detected in the NRAO VLA Sky Survey (NVSS). One of the three galaxies (MCG-03-34-04) is listed as a lenticular in literature, while the other two (UGC3004 and UGC3014) are listed as spirals with no further morphological specification. High resolution 20 cm GMRT maps of these three sources are presented in this chapter (Fig. 32, 33, 34). Table 3 lists the relevant parameters.

Five galaxies in this sample are FIR detected. The FIR luminosities were derived from the $60\mu m$ flux using the following relation [163].

$$\log L_{60\mu m}(L_{\odot}) = 6.014 + 2\log D + \log S_{60\mu m} \tag{3.6}$$

where $S_{60\mu m}$ is FIR $60\mu m$ flux density in Jy, D is the distance to the galaxy in Mpc and L is the $60\mu m$ FIR luminosity. For $S_{60\mu m}$, in all the five cases, IRAS (Infrared Astronomical Satellite) $60\mu m$ fluxes were used. The 20cm radio continuum luminosities were derived using [163]

$$\log L_{1.4GHz}(WHZ_1) = 20.08 + 2\log D + \log S_{1.4GHz} \tag{3.7}$$

where $S_{1.4GHz}$ is the radio 20cm flux density in Jy, D is the distance to the galaxy in Mpc and $L_{1.4GHz}$ is radio luminosity in 20 cm. For the two FIR detected but radio non-detected galaxies (ARP004 and MCG-03-34-41), 3σ radio upperlimit fluxes were used in calculating their luminosities. The three galaxies which are detected both in radio and FIR follow the FIR-radio correlation. The radio non-detected galaxies deviate from the radio-FIR correlation to some extent. To quantify this deviation the Q parameter was calculated, using the following relation [32]

$$Q = \log(\frac{FIR}{3.75 \times 10^{12} Wm^{-2}}) - \log(\frac{S_{1.4GHz}}{1.0 \times 10^{26} Wm^{-2} Hz^{-1}}) \tag{3.8}$$

where $S_{1.4GHz}$ is the 20 cm radio flux density in Jy and FIR is calculated in the following manner [61]

$$FIR = 1.26 \times 10^{-14}(2.58 S_{60\mu m} + S_{100\mu m}) Wm^{-2} \tag{3.9}$$

The plot of Q versus $\log L_{60\mu m}$ (Fig 2), shows the three galaxies, detected both in radio and FIR, near the Q=2.34 line, which is the mean value of Q for spirals and irregulars [163]. The two dotted lines about the Q=2.34 line represent 3 times radio excess (bottom line) and 3 times radio deficit (top line) respectively. The two galaxies, ARP004 and MCG-03-34-41, represented with arrows for radio non-detection, close to the upper dotted line, tend to show they have excess FIR emission. Star formation rates of the three radio detected galaxies were calculated using [163]

$$SFR(M_\odot yr^{-1}) = 5.9 \pm 1.8 \times 10^{-22} L_{1.4GHz} WHz^{-1} \tag{3.10}$$

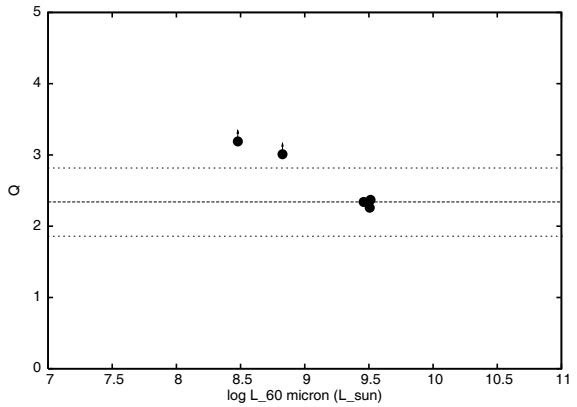

Figure 3.2: The 'Q' value plotted against $\log L_{60\mu m}(L_{\odot})$

where $L_{1.4GHz}$ is the radio luminosity in 20 cm, detected by GMRT. The star formation rates are normal in these galaxies ranging from $\sim$ 1 to 2 $M_{\odot}\ yr^{-1}$. The relevant parameters of the radio continuum and FIR properties of the five galaxies are listed in table 3.

3.4 Discussion

Environment affects the gas content and morphology of a galaxy as demonstrated by studies of cluster galaxies ([59], [24]). Different gas removal processes like ram pressure stripping, galaxy harassment ([93]), strangulation ([46]) and thermal conduction ([34]) can strip off gas from galaxies. Tidal interactions are less likely to work as an efficient gas removal mechanism in the cluster environment as the velocities with which the galaxies move past each other are very high. In groups, the environment is diffierent from the clusters. The IGM densities are often lower than the ICM densities and the velocity dispersion of the galaxies in groups are also lower than in clusters. The lower velocity dispersion helps tidal interactions to work better in groups and at the same time makes ram pressure stripping less efficient process than in clusters. An effort has been made here to estimate how much gas loss is possible through ram pressure stripping and thermal conduction, and to see whether that can explain the observed gas deficiency and shrunken H I disks.

3.4.1 Expected HI deficiencies

3.4.1.1 Ram Pressure

In cluster environments ram pressure stripping is seen to be an effective process for removing gas from galaxies. In groups this process was not considered to be an efficient one because of lower IGM density and lower velocity dispersion, both being smaller by an order of magnitude compared to clusters. These make direct ram pressure stripping effective only below a critical H I column density of 10^{19} per cm^2 for a normal galaxy with an optical radius of 10 kpc, and 10^{11} stars . However in X-ray bright groups this picture can be different. The dense X-ray gas in the central regions of the groups can strip off a large amount of neutral gas from the galaxies which move across these regions. A simple estimation is done here for all the H I detected galaxies to study the effect of ram pressure on them. Ram pressure stripping [58] is effective for a galaxy when the H I surface mass density is less than $\rho_0 v^2/(2\pi\ G\sigma_*)$, where σ_* is the stellar surface mass density, ρ_0 is the IGM density and v is the velocity with which the galaxy is moving through the medium. Stellar surface matter density for these galaxies were estimated using their K-band magnitudes and K-J colors. In the absence of K and J band data, other bands were used. The Mass to light ratio in K band (M/L_K) of the galaxies are related to the K-J colors by the formula [9]

$$log(M/L_K) = a_K + b_K\ color_{K-J} \tag{3.11}$$

Luminosity in K-band, L_K is related to the absolute magnitude in K-band (M_K) in the following way [162]

$$L_K(L_\odot) = \exp\left(0.921034\ (3.33 - M_K)\right) \tag{3.12}$$

Thus the stellar mass surface density (σ_*) for all the galaxies for which the necessary photometric observations were available, were estimated using their magnitude and color information. For ρ_0, the local IGM densities at the projected positions of the galaxies were used. Since all the groups in this sample do not have published density profiles for the IGM,

the local densities for those cases (NGC720 and IC1459) were taken to be an average of the densities at the galaxy positions of two well studied groups in X-rays, NGC1550 and NGC5044, which also belong to this sample ([139], [37]). The velocity dispersions of the groups were used as the velocities with which the galaxies are moving through the medium (v). For NGC1550 and NGC5044 the group velocity dispersions were taken from the literature ([139] and [25]). Such detailed study are not present for the groups NGC720 and IC1459. Therefore velocity dispersion for these two groups were derived using the IGM temperatures (T) found from the X-ray observations [97]. Thus dispersion for these groups is basically $\sqrt{\frac{3kT}{m_p}}$, where m_p is the proton mass and k is the Boltzmann constant. Thus the critical H I column density σ_μ, beyond which ram pressure is able to stirp off gas if a galaxy moves face on through the IGM, were calculated for these galaxies using

$$\sigma_\mu = \rho_0 \mathrm{v}^2/(2\pi\, G\sigma_*) \tag{3.13}$$

Assumimg the H I distribution to be of constant thickness and to be distributed in a Gaussian profile [28]

$$\sigma(r) = \sigma_0\, 2^{-r^2/r_H^2} \tag{3.14}$$

where r_H is the radius within which half the H I mass is present, the mass outside the radius of the critical H I column density (σ_μ), for a galaxy was calculated in the following way. The total expected H I mass ($M_{\mathrm{H_I}}$) of a galaxy (of a known size and a morphological type) was derived using the field values [59]. The r_H of equation 14. was then found by solving

$$\int_0^\infty 2\pi r\sigma(r)dr = M_{\mathrm{H_I}} \tag{3.15}$$

which simplifies to

$$r_H = \sqrt{\frac{2\log 2 M_{\mathrm{H_I}}}{2\pi\sigma_0}} \tag{3.16}$$

The next step was to find the H I radius (R) corresponding to the critical H I column density (σ_μ). This was done by solving

$$2^{-R^2/r_H^2} = \sigma_\mu/\sigma_0 \tag{3.17}$$

In the absence of the true peak H I column density (σ_0) values, the peak H I column density values of the GMRT total H I images were used, assuming that the central regions of the galaxies have been unaffected by the gas removing processes. Finally the H I mass (M_{lost}) outside the H I radius (R) corresponding to σ_μ was calculated by integrating the H I column density profile from R to ∞.

$$2\pi\sigma_0 \int_R^\infty r 2^{-r^2/r_H^2} dr = M_{lost} \tag{3.18}$$

The percentage mass loss by this process ($M_{lost}/M_{\rm H\,I}$) for all the galaxies for which the relevant data were available are listed in table 4, column 6.

However these estimates were done under the following assumptions,

- the galaxy is moving face-on through the IGM
- the position of the galaxy with respect to the group centre is same as the projected distance from the group centre
- the orbital history of the galaxy is not taken into account, i.e whether the galaxy has crossed the group centre or not.

These may explain why the individual H I deficiencies of the galaxies and their percentage ram pressure stripped gas do not necessarily match (table 4). Still these calculations show that ram pressure by itself or tidal aided ram pressure cannot be ruled out as important gas removing processes in the groups having a hot IGM.

3.4.1.2 Thermal conduction

Evaporation via thermal conduction is another process which is responsible for mass loss from galaxies embedded in a hot medium [34]. For classical, unsaturated thermal conduction

the rate of mass loss is

$$\dot{M} = 700 M_{\odot} yr^{-1} (\frac{T_{IGM}}{10^8})^{5/2} (\frac{R}{20kpc}) (\frac{\ln \Lambda}{40})^{-1} \tag{3.19}$$

where T_{IGM} is the IGM temperature in Kelvin, R is the radius of the galaxy and $\ln \Lambda$ is the Coulomb logarithm ([33], [150]). In these estimates, T_{IGM} values are taken from the X-ray observations of the groups, R is the optical size ($D_l/2$) of the galaxy and Coulomb logarithm is assumed to be unity. Mass loss possible through unsaturated thermal conduction in 1 Gyr is listed in table 4. Column 8 of table 4 lists the total expected H I deficiency values, a sum total of columns 6 and 7. These estimates are done under the following assumptions,

- thermal conduction has been considered to be unsaturated
- the galaxies are embedded in the same temperature for 1 Gyr
- there is no effect of magnetic fields in supressing the mass loss rate

Because of these assumptions, these estimates may not necessarily reflect the true gas loss for the galaxies through this process. In practice thermal conduction is saturated on galaxy scales, as the mean free path of the electrons in the hot plasma is comparable to the size of a galaxy. Saturated thermal conduction along with the local magnetic fields will reduce the gas loss through thermal conduction significantly. Also the assumption that the galaxies are embedded in the same temperature for 1 Gyr, may not be always correct. However, within these limitations, these calculations demonstrate that under some reasonable assumptions, ram pressure stripping and in some cases thermal conduction can actually strip off gas from galaxies in these groups.

3.4.2 Observed H I properties

The galaxies were observed with the aim to study their H I morphology and to see if IGM assisted gas stripping has left any signature on their H I distribution. The H I deficiency estimated for each H I detected galaxy (eqn.4) are listed in table 4. Most of the galaxies which

are reasonably H I deficient, by about a factor of 2 or more, show distorted H I morphology. DDO015 is H I deficient by a factor of 9, and the total H I image of this galaxy shows that gas is mostly present in the eastern region. Part of western and central region of this galaxy has depleted gas content. For SGC1317.2-1702 H I distribution is clumpy and fragmented. This galaxy is deficient by a factor of 3. ARP004 is not a H I deficient galaxy, but shows an extremely fragmented H I structure in the high resolution map (Fig. 5). But in a lower resolution map the galaxy looks very different with a normal H I distribution (Fig. 3). However this is the only case where the high and low resolution maps look very different and therefore both the maps are presented. Another interesting galaxy in this sample is MCG-03-34-04. This is classified as a lenticular(S0) in literature. Lenticulars normally do not contain much H I . An average field lenticular of this size is expected to contain an H I mass of 1.8×10^9 $M_\odot$ whereas this galaxy has a H I mass of about 8×10^9 $M_\odot$.

The ratio D_{Hi}/D_{25}, also gives an idea of gas loss from galaxies. The average value of D_{Hi}/D_{25} for spirals and irregulars in the field has been found to be 1.7 ± 0.8. The average of the current sample is 1.1±0.12, with most galaxies having a value close to 1.0 (table 4). This points towards the possibility of ram pressure stripping off the low column density gas from the outer edges of the galaxies. Since these galaxies belong to groups where velocity dispersion is low enough to allow tidal interactions, tidal aided ram pressure stripping can also remove gas from the galaxies [39]. In this case tidal interaction can stretch the gas below the critical H I column density and then even a mild ram pressure can strip off the extended low column density gas from the galaxies. All these mechanisms can give rise to shrunken or truncated H I disks. MCG-03-34-41 is a spiral galaxy deficient in H I by a factor of 3. The H I morphology of this galaxy seems to be apparently normal (Fig.10) other than the fact that its D_{Hi}/D_{25} value is 1.1, which is significantly less than galaxies with normal gas content. The plot of H I deficiency versus D_{Hi}/D_{25} (Fig. 1), indicates that D_{Hi}/D_{25} is smaller for galaxies with higher H I deficiency.

3.5 Conclusion

A single dish comparative study revealed that galaxies in X-ray bright groups have lost more gas on average than the galaxies in non X-ray bright groups. To study if the hot IGM is responsible for gas stripping from these galaxies, 13 galaxies from 4 X-ray bright groups were imaged in H I with GMRT. Disturbed H I morphology was seen in some cases but most galaxies were seen to have a shrunken H I disk. This indicates that ram pressure may have stripped gas from the outer edges of the galaxies. In a group environment where tidal interactions can work better than in clusters and ram pressure alone cannot strip gas as efficiently as in clusters, tidal aided ram pressure can strip off gas from the outer edges of the galaxies, giving rise to apparently undisturbed but shrunk H I disks.

Table 3.2: GMRT Observations

Galaxy	Coordinate (J2000)	Optical Velocity (km/s)	M type	τ (Hrs)	BW (MHz)	rms/channel (mJy/beam)	beam (") (total H I)	beam (") (velocity field) & PA (deg)
Arp004	01 48 25.7 -12 22 55	1614	Im	3.2	4.0	1.50	20.0"×20.0"	–
				3.2	4.0	2.00	46.7"× 38.9"	– 46.7"×38.9" -29.1
DDO015	01 49 40.2 -12 49 27	1710	Sm	3.2	4.0	0.90	20.0"×20.0"	20.0"×20.0" –
UGC3004	04 17 19.0 +02 26 00	3571	S(?)	3.6	8.0	1.00	13.0"×13.0"	13.0"×13.0" –
UGC3005	04 17 20.5 +02 27 01	3215	Scd	3.6	8.0	1.00	13.0"×13.0"	13.0"×13.0" –
UGC3006	04 17 25.3 +02 22 16	3664	S0	3.6	8.0	1.00	–	– –
UGC3014	04 19 53.7 +02 05 36	4214	S(?)	6.0	4.0	0.57	15.0"×15.0"	37.7"×29.7" -36.4
MCG-03-34-41	13 17 06.1 -16 15 08	2651	Sc	3.0	4.0	1.20	20.0"×20.0"	20.0"×20.0" –
MCG-03-34-04	13 09 44.1 -16 36 08	2619	S0	3.3	8.0	0.63	25.0"×25.0"	44.9"×34.8" -12.3
NGC4997	13 09 51.7 -16 30 56	2376	S0	3.3	8.0	0.63	–	– –
SGC1316.2-1722	13 18 56.5 -17 38 06	2495	Sm	2.6	4.0	0.96	20.0"×20.0"	56.1"×35.1" -15.1
SGC1317.2-1702	13 19 54.8 -17 18 56	2689	Sdm	3.0	4.0	1.20	20.0"×20.0"	20.0"×20.0" –
NGC5031	13 14 03.2 -16 07 23	2839	S0	3.3	8.0	0.70	–	– –
IC5269B	22 56 36.7 -36 14 59	1667	Scd	3.5	4.0	0.80	20.0"×20.0"	56.4"×27.7" -19.6

M type : Morphological type, τ : Integration time, PA : Position Angle, BW : Bandwidth

Table 3.3: GMRT Continuum observations

Galaxy	Total Flux Density from GMRT (mJy)	rms (mJy/beam)	beam size (")	PA (deg)	Log of Radio Luminosity (WHz^{-1})	Log of FIR ($60\mu m$) Luminosity ($L_\odot$)	FIR ($100\mu m$) Flux (Jy)	Q
UGC3004	10.67	0.09	4.0"×4.0"	–	21.46	9.51	3.85	2.37
UGC3014	6.5	0.25	13.1"×10.7"	46.9	21.39	9.46	2.00	2.34
MCG-03-34-04	21.79	0.16	6.2"×2.6"	-11.2	21.50	9.51	5.21	2.26
ARP004	< 0.81	0.27	4.0"×4.0"	–	<19.68	8.48	2.33	3.19
MCG-03-34-41	<0.78	0.26	8.2"×5.0"	-84.1	<20.07	8.83	1.05	3.01

Table 3.4: Observed and estimated parameters

Galaxy	angular diameter(')	HI mass ($M_\odot$)	H I deficiency	D_{HI}/D_{25}	Ram pressure % stripped	Evaporation in 1Gyr ($M_\odot$)	expected H I deficiency
Arp004	2.8	1.95×10^9	0.15	–	34.4	1.7×10^8	0.23
DDO015	1.9	1.80×10^8	0.90	0.6	54.3	7.7×10^7	0.39
U3004	1.2	8.99×10^8	0.40	0.9	1.6	2.0×10^9	0.97
U3005	1.2	1.56×10^9	0.12	1.6	–	1.8×10^9	–
U3014	1.2	2.34×10^9	0.13	1.2	4.0	2.3×10^9	0.64
MCG-03-34-41	2.3	1.66×10^9	0.40	1.1	6.0	1.4×10^9	0.21
MCG-03-34-04	1.9	8.00×10^9	-0.64	1.8	–	–	–
SGC 1316.2-1722	2.0	1.07×10^9	0.49	0.8	–	1.1×10^9	–
SGC 1317.2-1702	1.9	1.09×10^9	0.51	0.8	–	1.1×10^9	–
IC5269B	4.1	2.37×10^9	0.42	1.1	65.0	4.6×10^8	0.56

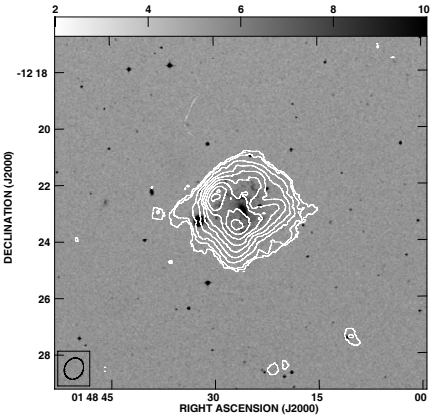

Figure 3.3: Total H I map (low resolution) : Arp004. The column density contours=1.8E+19/cm^2×(3, 5, 10,15, 20, 25, 30, 35, 40)

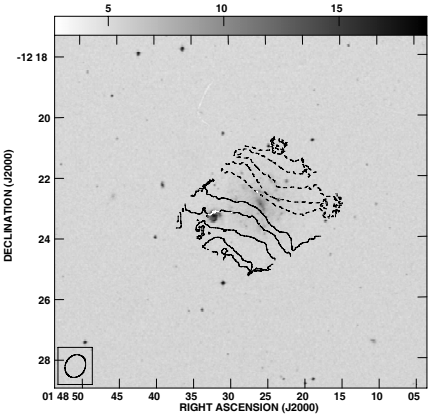

Figure 3.4: H I velocity field : Arp004. The velocity contours in km/s=1.0E+03×(-50, -40, -30, -20, -10, 10, 20, 30, 40, 50)

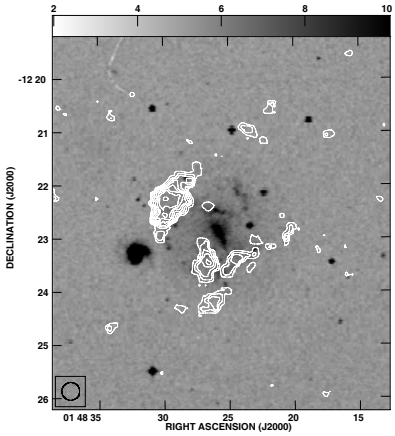

Figure 3.5: Total H I map (high resolution) : Arp004. The column density contours=3.3E+19/cm^2×(3, 5, 7, 9, 11, 13, 15, 20)

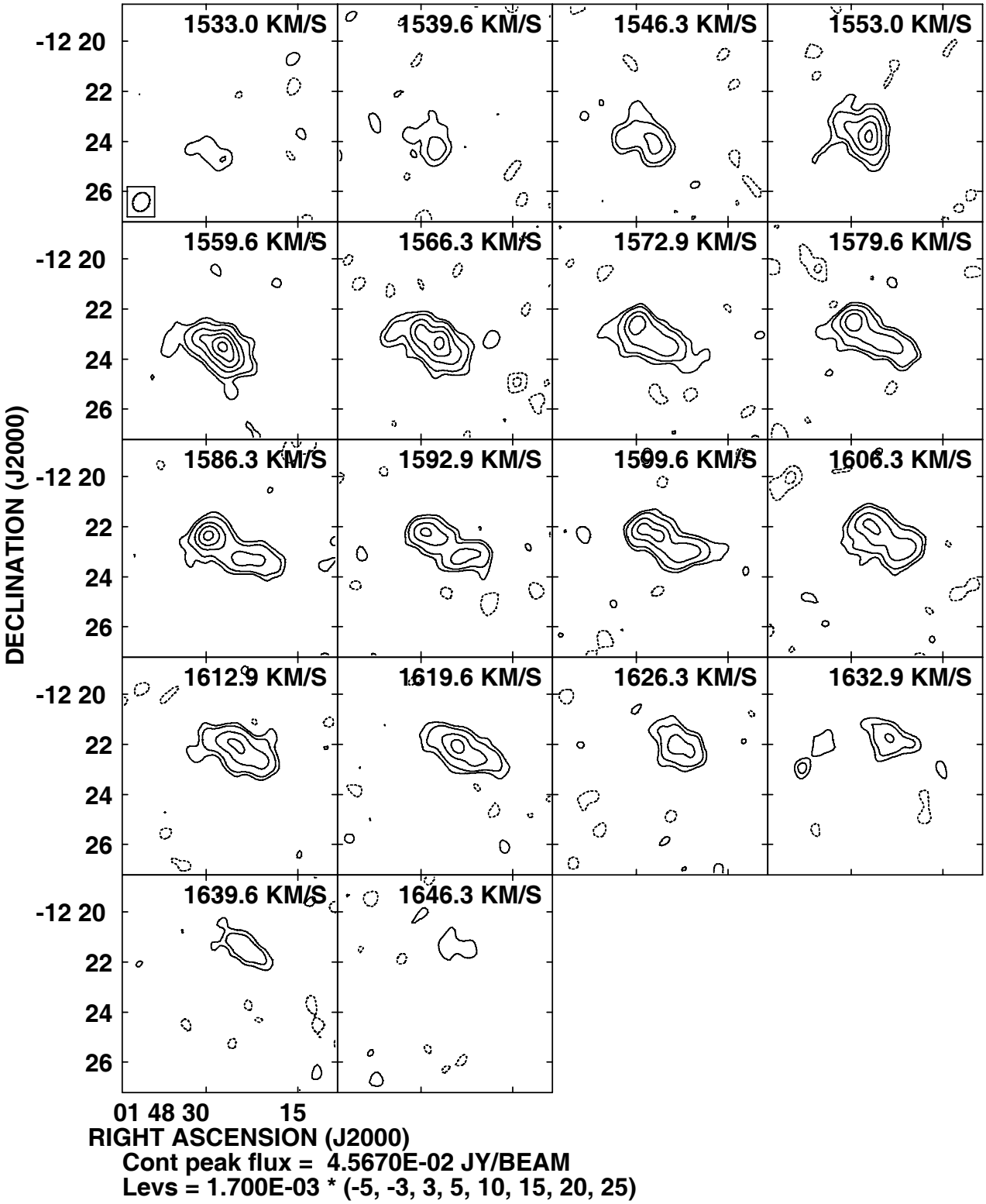

Figure 3.6: Channel maps for Arp004

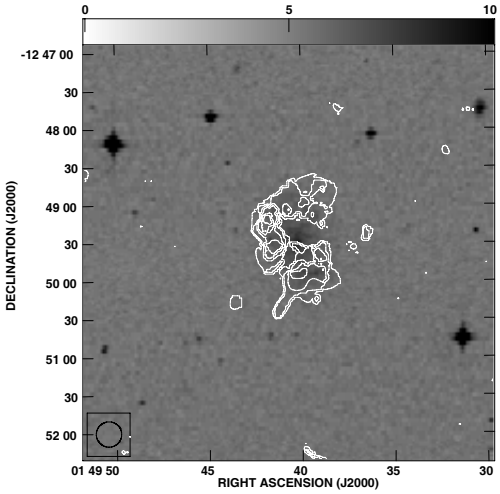

Figure 3.7: Total H I map : DDO015. The column density contours=4.4E+19/cm^2×(3, 5, 7, 9, 11, 13, 15)

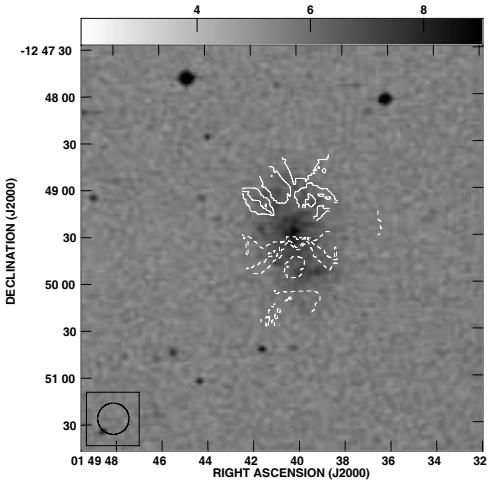

Figure 3.8: H I velocity field : DDO015. The velocity contours in km/s=1.0E+03×(-40, -30, -20, -10, 10, 20, 30, 40)

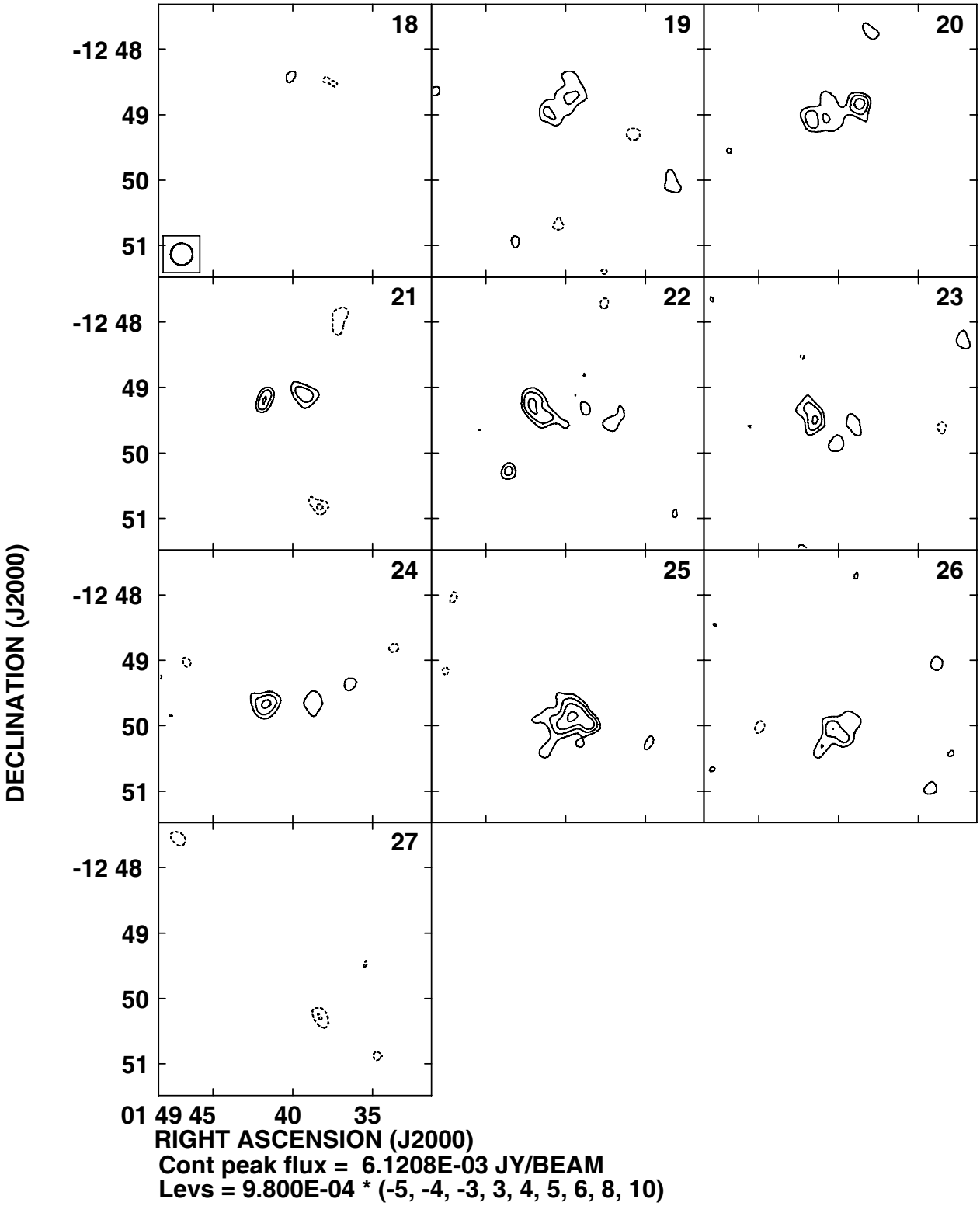

Figure 3.9: Channel maps for DDO015

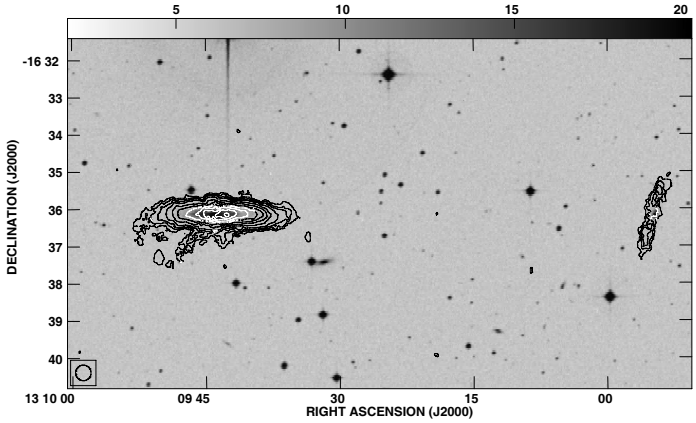

Figure 3.10: Total H I map : MCG-03-34-04. The column density contours=4.4E+19/cm^2×(3, 5, 7, 10, 15, 20, 25, 30, 35, 40, 45, 50)

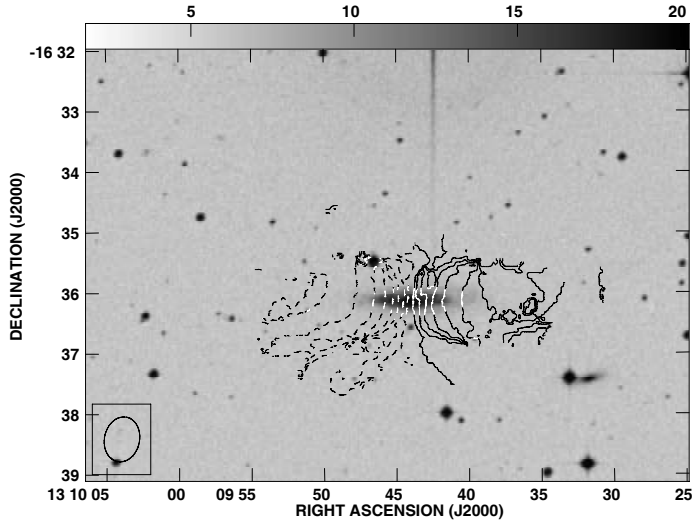

Figure 3.11: H I velocity field : MCG-03-34-04 : The velocity contours in km/s=1.0E+03×(-170, -160, -140, -120, -100, -80, -60, -40, -20, 20, 40, 60, 80, 100, 120, 130, 140)

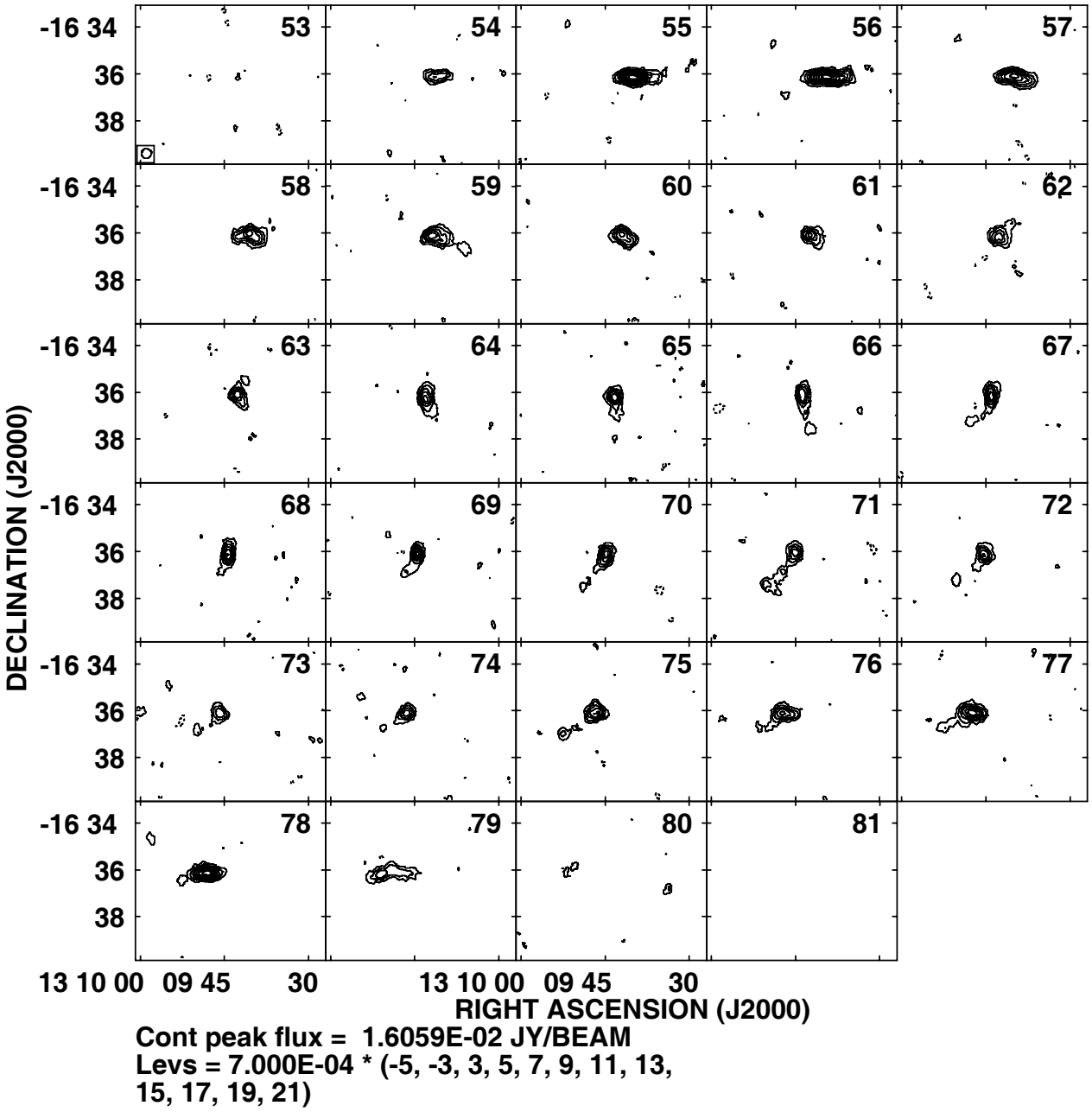

Figure 3.12: Channel maps for MCG-03-34-04

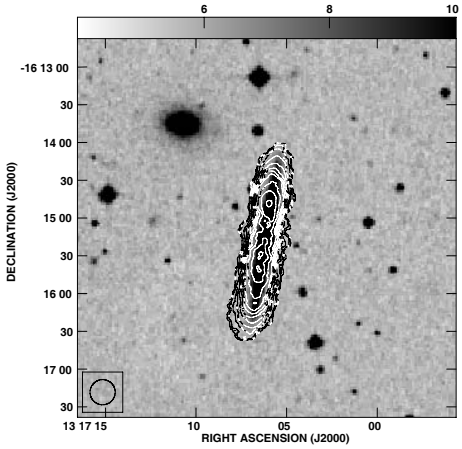

Figure 3.13: Total H I map : MCG-03-34-41 : H I column density=4.1E+19/cm^2×(3, 5, 10, 15, 20, 25, 30, 35, 45, 55, 65)

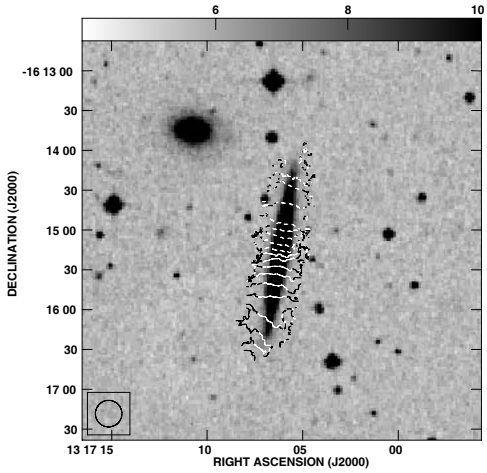

Figure 3.14: H I velocity field : MCG-03-34-41 : H I velocity contours in km/s=1.0E+03×(-135, -125, -115, -95, -75, -55, -35, -15, -5, 5, 15, 35, 55, 75, 95, 115, 125, 135)

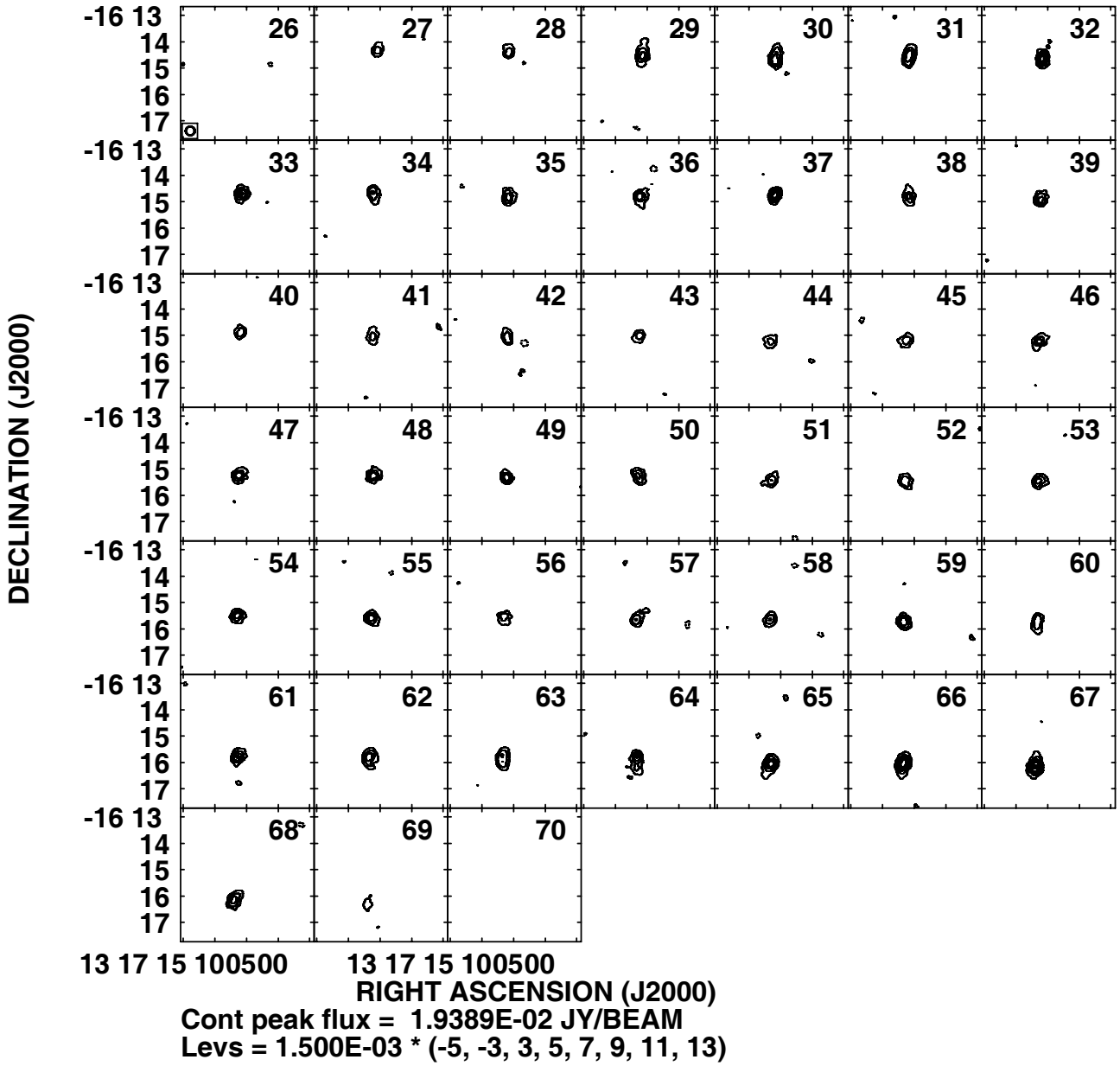

Figure 3.15: Channel maps for MCG-03-34-41

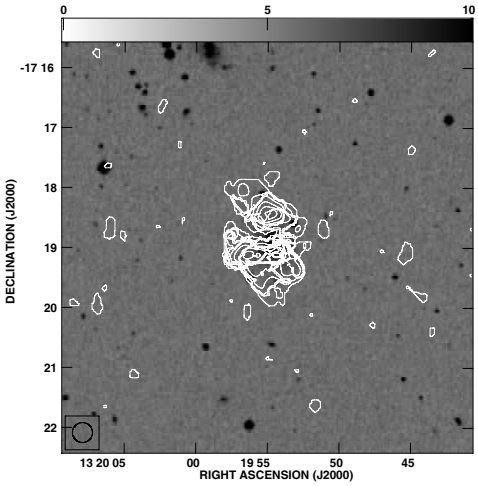

Figure 3.16: Total H I map : SGC1317.2-1702. The column density contours=4.4E+19/cm^2×(3, 5, 7, 9, 11, 13, 15, 17, 19, 21, 23)

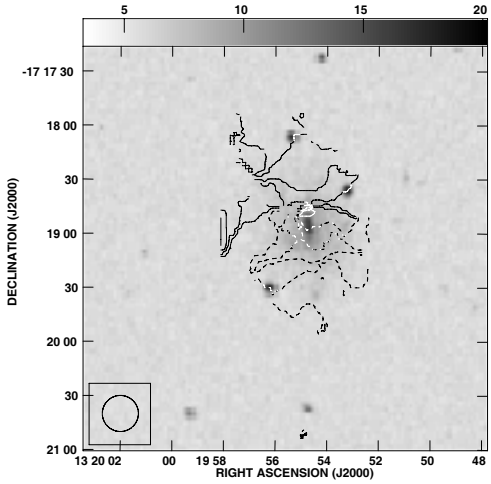

Figure 3.17: H I velocity field : SGC1317.2-1702. The velocity contours in km/s=1.0E+03×(-50, -40, -30, -20, -10, 10, 20, 30, 40, 50)

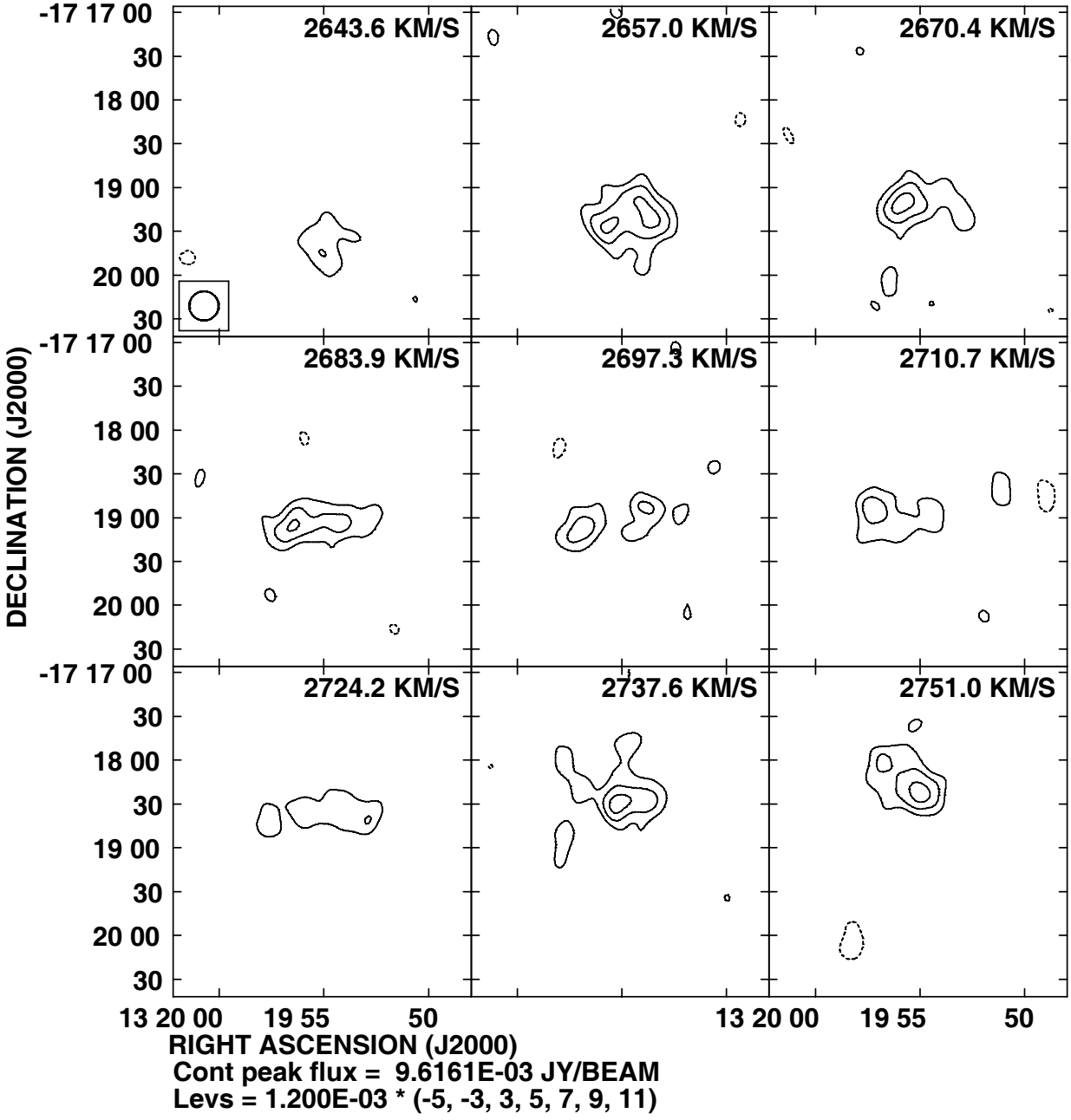

Figure 3.18: Channel maps for SGC1317.2-1702

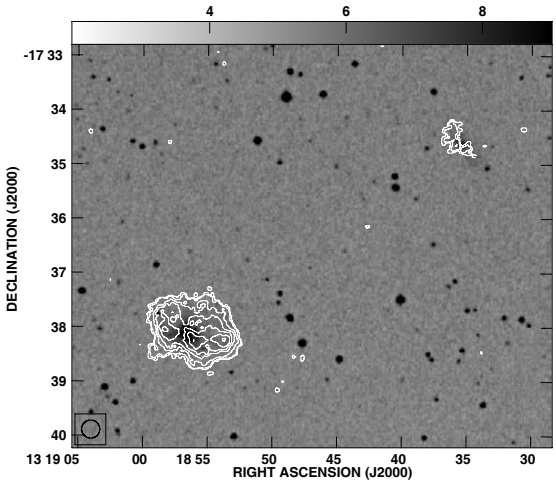

Figure 3.19: Total H I map : SGC1316.2-1722. The column density contours=2.8E+19/cm^2×(3, 5, 10, 15, 20, 25, 30)

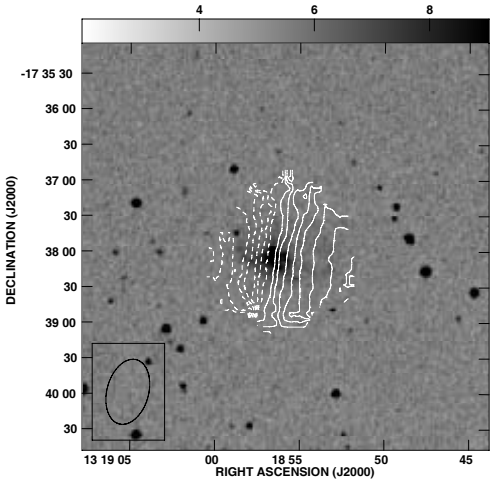

Figure 3.20: H I velocity field : SGC1316.2-1722. The velocity contours in km/s=1.0E+03×(-35, -30, -25, -20, -15, -10, -5, 5, 10, 15, 20, 25, 30, 35, 40)

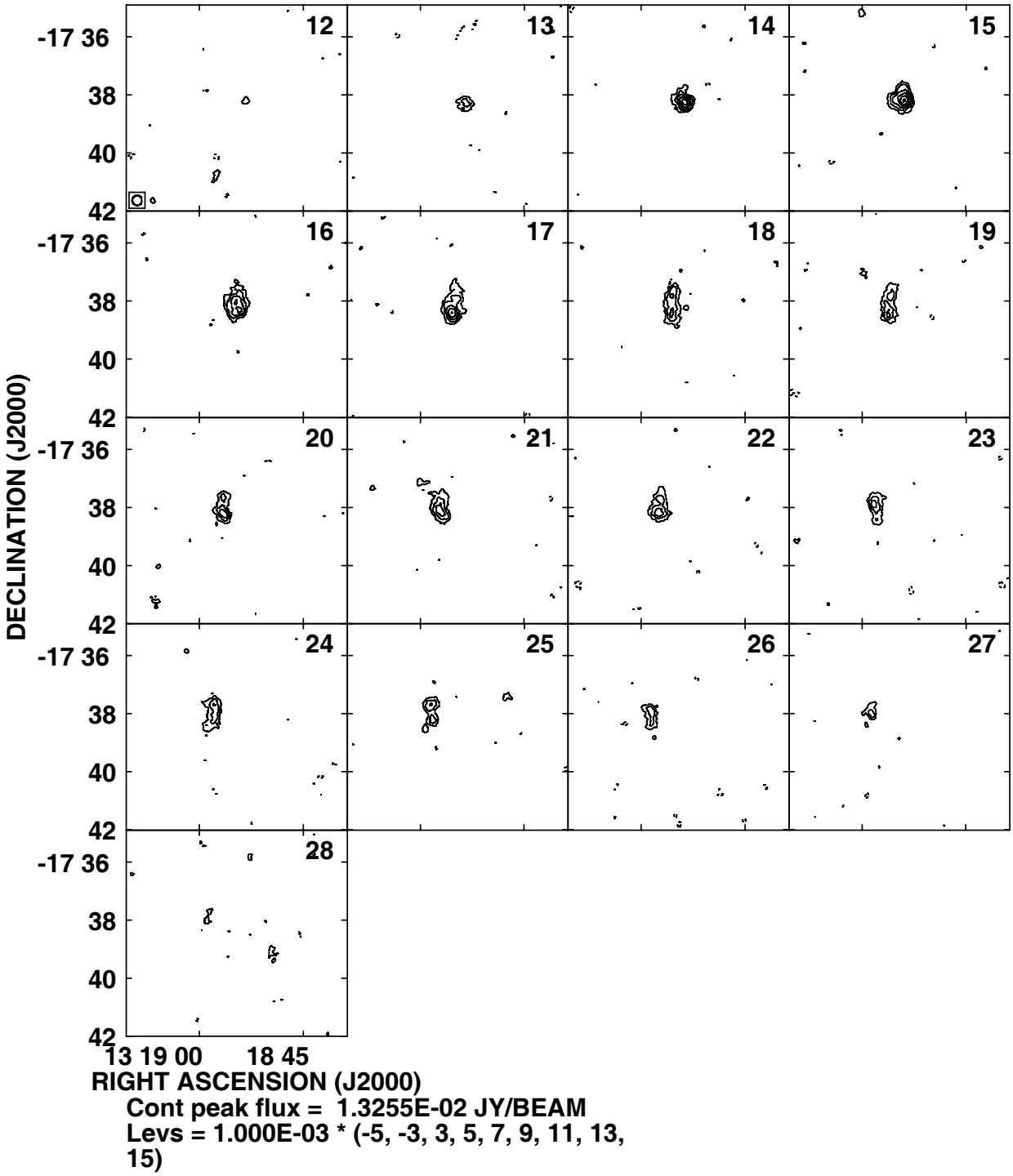

Figure 3.21: Channel maps for SGC1316.2-1722

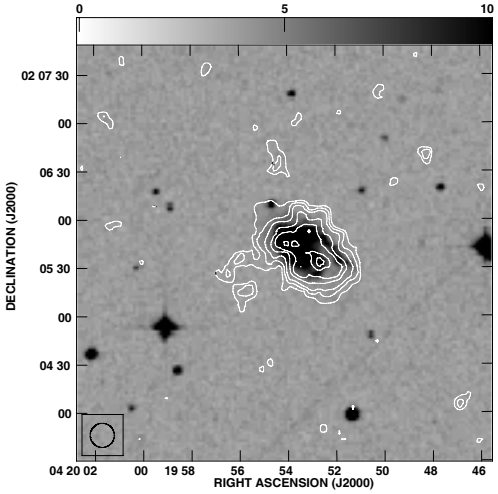

Figure 3.22: Total H I map : UGC3014. The column density contours=1.4E+20/cm^2×(3, 5, 7, 10, 12, 15, 17)

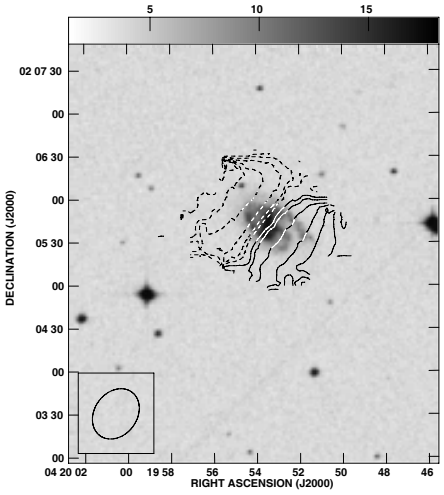

Figure 3.23: H I velocity field : UGC3014. The velocity contours in km/s=1.0E+03×(-110, -100, -80, -70, -60, -40, -20, -10, 10, 20, 40, 60, 70, 80, 100, 110)

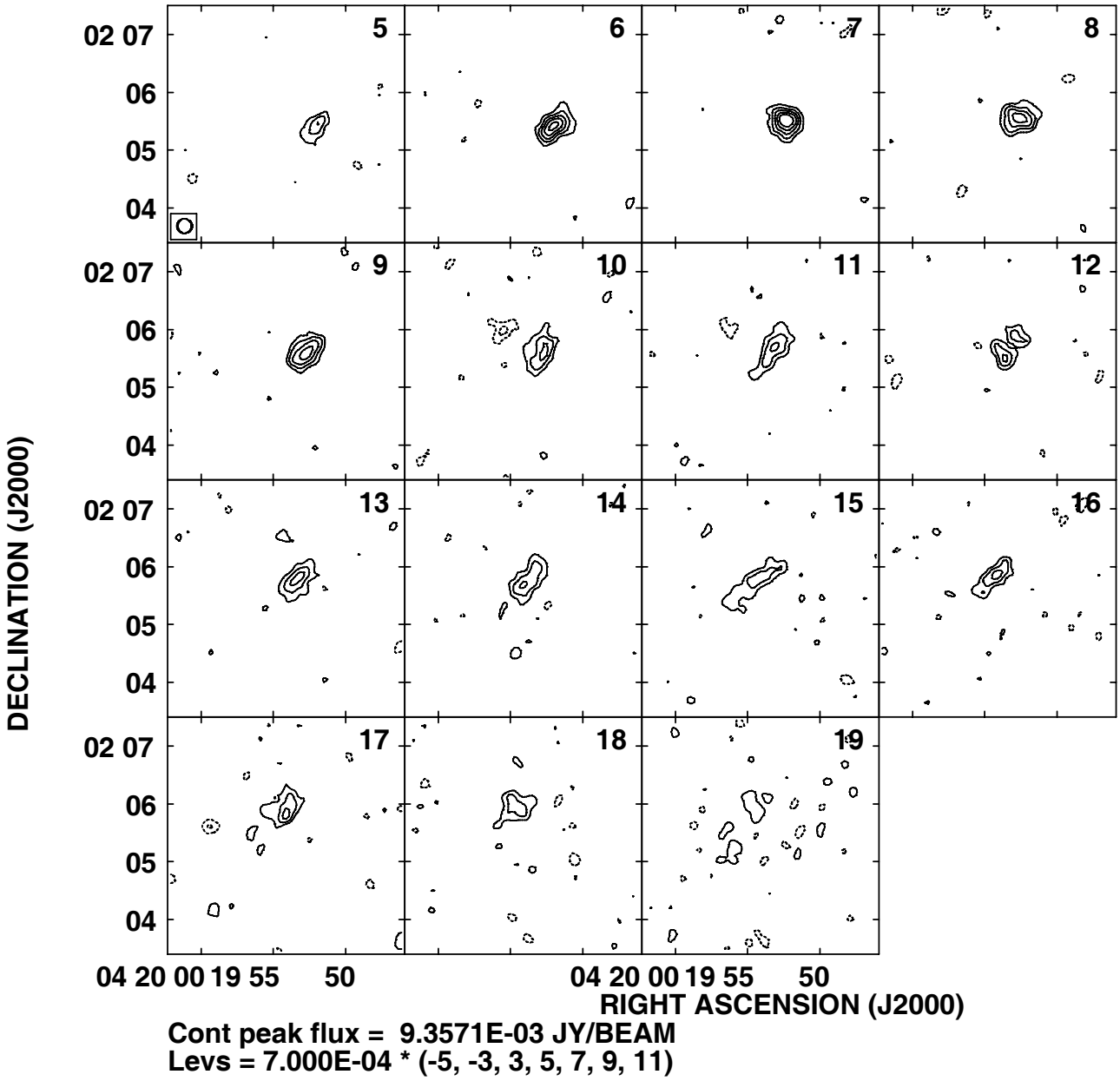

Figure 3.24: Channel maps for UGC3014

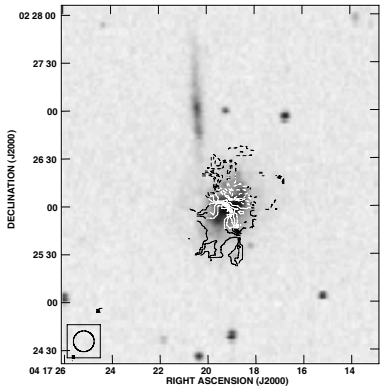

Figure 3.25: H I velocity field : UGC3004. The velocity contours in km/s=1.0E+03×(-70, -60, -50, -40, -30, -20, -10, 10, 20, 30, 40, 50, 60, 70)

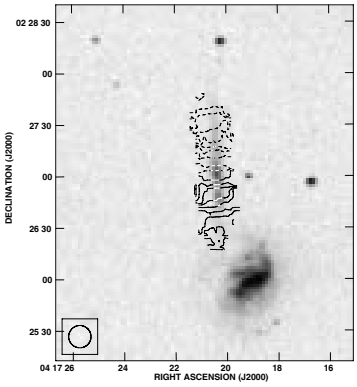

Figure 3.26: H I velocity field : UGC3005. The velocity contours in km/s=1.0E+03×(-100, -90, -80, -70, -60, -50, -40, -30, -20, -10, 10, 20, 30, 40, 50, 60, 70, 80, 90, 100)

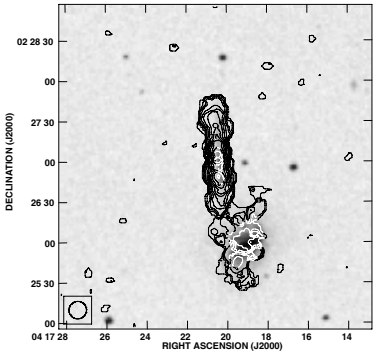

Figure 3.27: Total H I map : UGC3004 and UGC3005. The column density contours=9.1E+19/cm^2×(3, 5, 7, 10, 15, 20, 25, 30, 35, 40, 45, 50, 55)

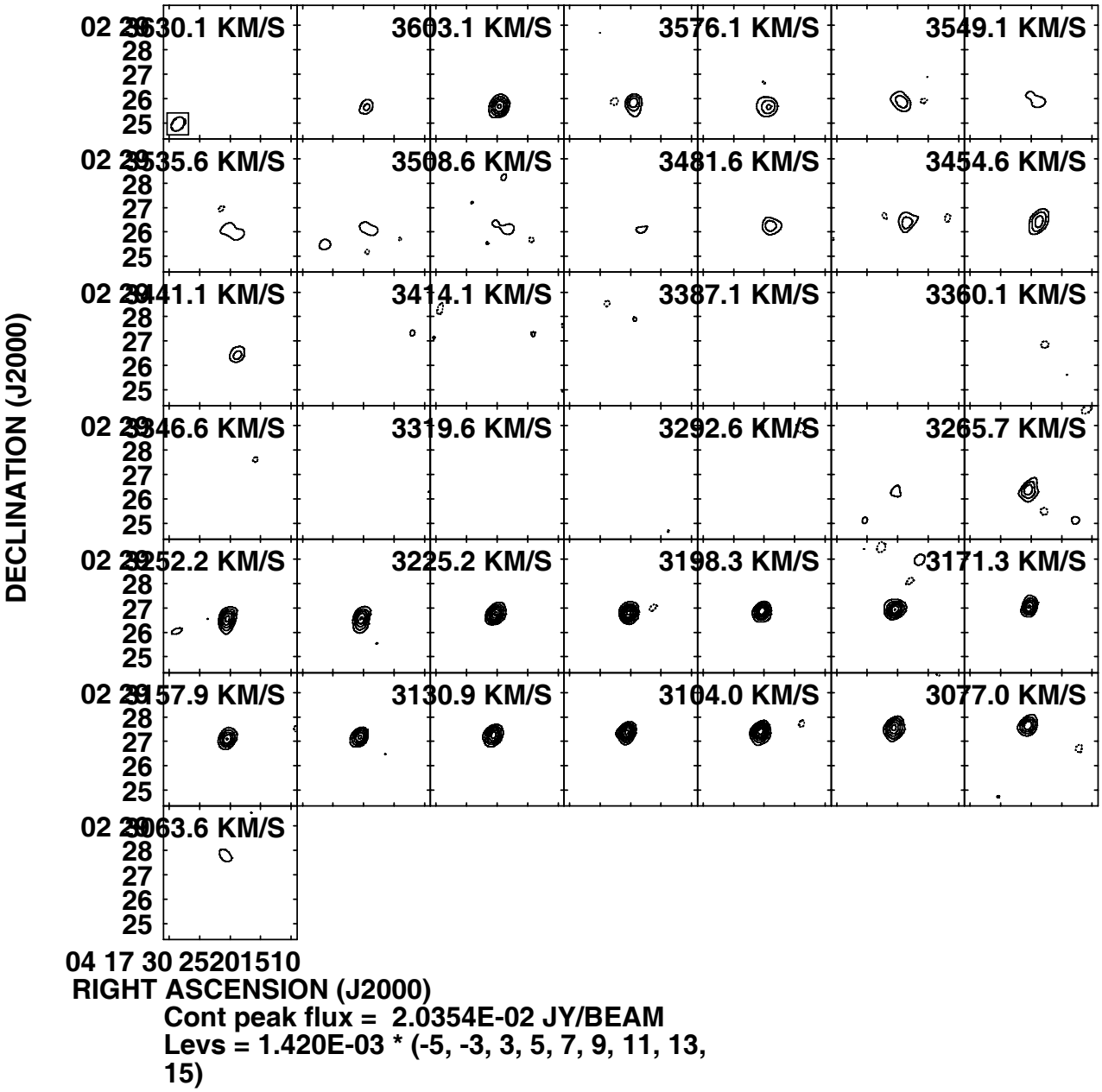

Figure 3.28: Channel maps for UGC3004 and UGC3005

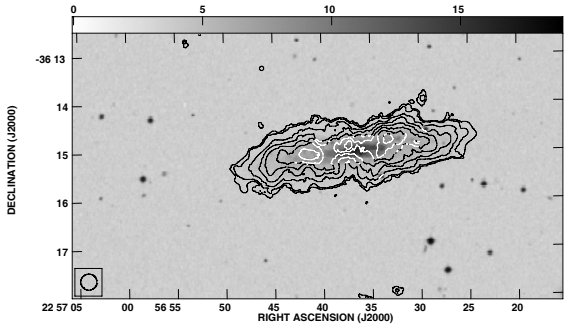

Figure 3.29: Total H I map : IC5269B. The column density contours=5.5E+19/cm^2×(3, 5, 10, 15, 20, 25, 30, 35)

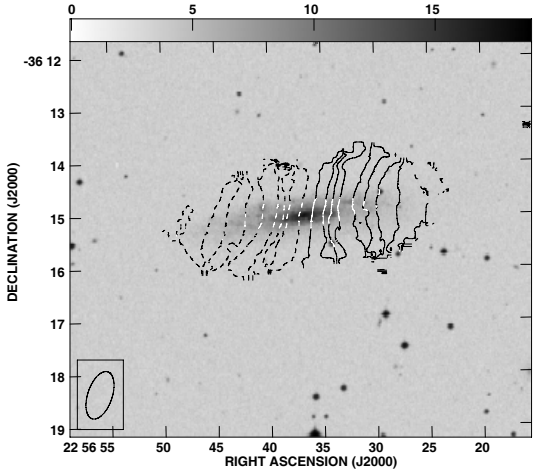

Figure 3.30: H I velocity field : IC5269B. The velocity contours in km/s=1.0E+03×(-110, -100, -90, -80, -70, -50, -40, -30, -10, 10, 30, 40, 50, 70, 80, 90, 100, 110)

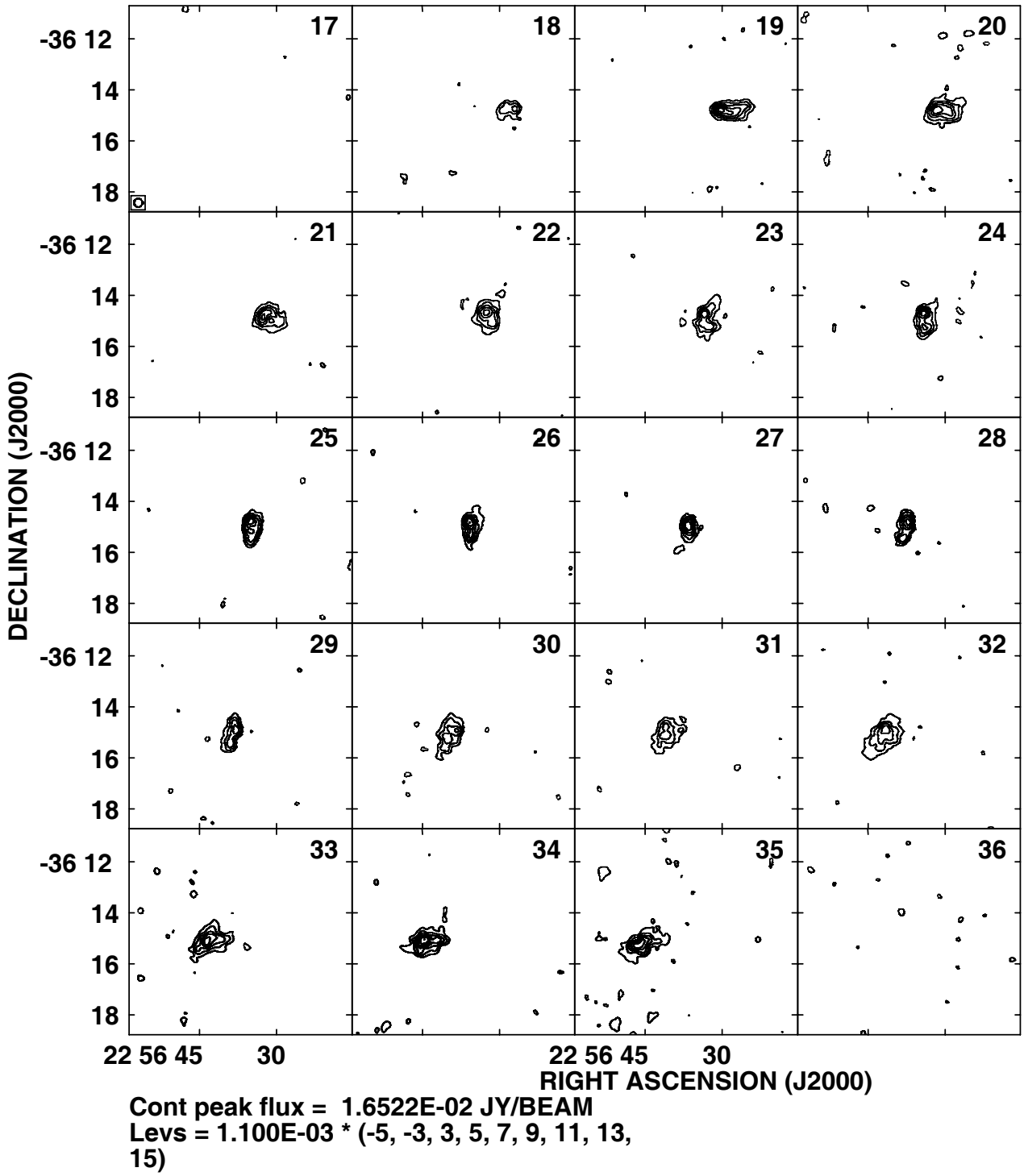

Figure 3.31: Channel maps for IC5269B

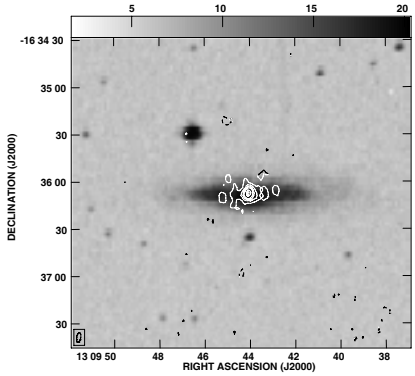

Figure 3.32: 20 cm radio continuum for MCG-03-34-04 contour levels = 1.500E-04 Jy×(-5, -3, 3, 5, 7, 9, 13, 15)

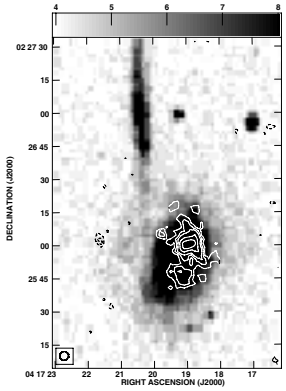

Figure 3.33: 20 cm radio continuum for UGC3004 contour levels = 8.000E-05 Jy × (-5, -4, -3, 3, 4, 5, 7, 9)

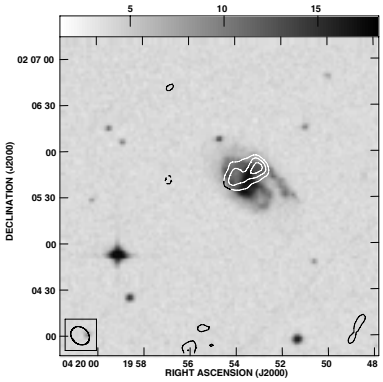

Figure 3.34: 20 cm radio continuum for UGC3014 contour levels = 2.500E-04 JY × (-5, -3, 3, 4, 5, 6, 7)